LA-UR- 10-08227

Approved for public release; distribution is unlimited.

Title:	Ultrafast Optical Control of Terahertz Surface Plasmons in Subwavelength Hole-Arrays at Room Temperature
Author(s):	Abul K Azad Hou-Tong Chen Antoinette J. Taylor John F. O'Hara
Intended for:	SPIE Photonics West

Los Alamos
NATIONAL LABORATORY
EST. 1943

Form 836 (7/06)

Ultrafast Optical Control of Terahertz Surface Plasmons in Subwavelength Hole-Arrays at Room Temperature

Abul K. Azad[1], Hou-Tong Chen[1], Antoinette J. Taylor[1], Weili Zhang[2], and John F. O'Hara[1]
[1]*MPA-CINT, Los Alamos National Laboratory, Los Alamos, NM-87545*
[2]*School of Electrical and Computer Engineering, Oklahoma State University, Stillwater, OK-74078*
Email: aazad@lanl.gov

Abstract

Extraordinary optical transmission through subwavelength metallic hole-arrays has been an active research area since its first demonstration. The frequency selective resonance properties of subwavelength metallic hole arrays, generally known as surface plasmon polaritons, have potential use in functional plasmonic devices such as filters, modulators, switches, etc. Such plasmonic devices are also very promising for future terahertz applications. Ultrafast switching or modulation of the resonant behavior of the 2-D metallic arrays in terahertz frequencies is of particular interest for high speed communication and sensing applications. In this paper, we demonstrate optical control of surface plasmon enhanced resonant terahertz transmission in two-dimensional subwavelength metallic hole arrays fabricated on gallium arsenide based substrates. Optically pumping the arrays creates a conductive layer in the substrate reducing the terahertz transmission amplitude of both the resonant mode and the direct transmission. Under low optical fluence, the terahertz transmission is more greatly affected by resonance damping than by propagation loss in the substrate. An ErAs:GaAs nanoisland superlattice substrate is shown to allow ultrafast control with a switching recovery time of ~10 ps. We also present resonant terahertz transmission in a hybrid plasmonic film comprised of an integrated array of subwavelength metallic islands and semiconductor holes. A large dynamic transition between a dipolar localized surface plasmon mode and a surface plasmon resonance near 0.8 THz is observed under near infrared optical excitation. The reversal in transmission amplitude from a stopband to a passband and up to $\pi/2$ phase shift achieved in the hybrid plasmonic film make it promising in large dynamic phase modulation, optical changeover switching, and active terahertz plasmonics.

1 Introduction

Extraordinary transmission of electromagnetic waves through periodic array of subwavelength holes has attracted enormous interest in both the understanding of its origin and the fascinating applications in a variety of fields since their experimental demonstration in the optical frequency regime[1]. Subwavelength metallic hole arrays have also obtained considerable attention regarding extraordinary optical transmission at terahertz (THz) frequencies[2-6]. Optical transmission efficiency of such arrays can be higher than unity when normalized by the holes' areas, and this anomalously high transmission has been explained as a result of resonance excitation of surface plasmon polaritons (SPPs) or surface plasmons (SPs) at the metal-dielectric interface. Surface plasmons polaritons (SPPs) are collective excitations for quantized oscillations of electrons[7]. The resonant interaction between electron-charged oscillations near the surface of metal and the electromagnetic field creates SPPs and results in rather unique properties[8]. SPP resonance is of particular interest at terahertz frequency because of the deficiency of natural materials to obtain a functional response at terahertz frequency. The so-called "THz gap" has resulted in the general failure to translate technologies from microwave and optical frequencies to the THz frequency range[9]. Artificially structured composite materials are playing an increasingly important role in overcoming the deficiency of natural materials at THz regime. The recent progress in subwavelength metallic hole arrays[2-6], THz metamaterials [9-11], and photonic crystals[12-14] may ultimately result in a complete manipulation of THz waves.

Experimental results have indicated that at optical frequency the SP-enhanced light transmission through subwavelength metallic hole arrays is normally achieved for metals with large ratio of the real to the imaginary dielectric constant, $-\varepsilon_{rm}/\varepsilon_{im} >> 1$ [15,16]. Notably, the conductivity of the metals at optical frequency is very poor even for the good conducting metals[17]. The ratio of dielectric constants, $-\varepsilon_{rm}/\varepsilon_{im}$, is generally higher for good conducting metals at optical frequency and indicate the conductive nature of metals. On the other hand, the conductivities of metal at terahertz regime almost retain their DC values and the ratio becomes $-\varepsilon_{rm}/\varepsilon_{im} < 1$ for non-transition metals, such as Ag, Au, Cu, and Al[17]. This was considered as a limitation to realize resonant

excitation of terahertz SPs in the periodic subwavelength structures. The recent studies, however, have demonstrated that an appropriate surface corrugation provided by the subwavelength structures could facilitate the resonant excitation of SPs even with $-\varepsilon_{rm}/\varepsilon_{im} < 1$ [18]. For the normal incident, the wavelength of the fundamental SPPs resonance mode of square lattice arrays can be written as[2,6],

$$\lambda_{Res} = L\sqrt{\frac{\varepsilon_1\varepsilon_2}{\varepsilon_1+\varepsilon_2}} \qquad (1)$$

where, L is the lattice parameter of the metal hole array and ε_1 is the dielectric constant of the dielectric medium and ε_2 is the dielectric constant of the metal. The enhanced transmission exceeds the geometrical transmission[1], and is orders of magnitude higher than that expected for non-resonant transmission through sub-wavelength holes[19].

The frequency selective resonance properties of subwavelength metallic hole arrays and metamaterials have potential use in functional THz devices such as filters, modulators, and switches[20-22]. Ultrafast switching or modulation of the resonant behavior of the terahertz metallic arrays is of particular interest for high speed communication and sensing applications. Switching of the SPP-assisted resonant THz transmission has been demonstrated using electric, optical, thermal, and magnetic techniques[20-24]. In these demonstrations either the dielectric properties of the substrates or the metallic grating were modified by external controls. For example, the conductivities of the metallic semiconductor gratings were controlled by either temperature or the applied optical excitation. In another demonstration, a magnetic field was applied to change the dielectric constant of the liquid crystal in the metal array[24]. Most of these methods do not support modulation on an ultrafast time scale. Hendry et al. [26] has applied an optical technique on a silicon-based metallic grating that supports fast modulation but only at cryogenic temperatures (20 K). Also their resonance recovery, or switching time, was about 100 ps at 20 K. In the case of optical modulation, switching time is mainly determined by the carrier lifetime of the substrate semiconductors. At room temperature, bulk silicon has a carrier lifetime of about a millisecond which severely degrades switching speed. Ultrafast switching recovery of surface plasmons (SP) resonance at the room temperature still remains a challenge to overcome.

In this work, we present the room temperature, ultrafast modulation of SPP-assisted THz transmission through a metallic grating fabricated on a GaAs-based ErAs:GaAs superlattice using ultrafast optical excitation. Due to the direct bandgap at 800 nm and the short carrier lifetime of this superlattice the SPP resonance can be modulated with much lower optical fluence than in[26] and can fully recover within ~10 ps at room temperature. We also present a large dynamic transition between a dipolar localized surface plasmon mode and a surface plasmon resonance at terahertz frequency observed under near infrared optical excitation. The presentation is organized as follows: in section II, we describe experimental methods of optical pump-terahertz probe spectroscopy. Section III describes the ultrafast switching of surface plasmons resonances. In section IV, we review the large dynamic transitions between surface plasmon resonance and localized surface plasmon resonance. Finally, section V gives a conclusive remark.

II Experimental setup

The SPP samples were characterized using a broadband optical-pump terahertz-probe (OPTP) terahertz time domain spectrometer (TDS). The terahertz TDS utilizes a 1kHz regeneratively amplified Ti:sapphire laser capable of generating 3.2 mJ, 50 fs pulses at 800 nm. Part of the output laser power is used for terahertz generation and detection using ZnTe crystals via optical rectification and the electro-optic effect[27, 28]. The remainder of the optical power passes through a variable attenuator to form a ~10 mm diameter illumination spot on the sample with an incidence angle of ~10°. Generated THz pulses from the transmitting ZnTe crstal are collimated and redirected to the detection ZnTe crystal by two pairs of parabolic mirrors. The samples are placed in between two inner parabolic mirrors where a THz beam waist of 3.5 mm is formed. The SPP sample and reference were placed at the THz beam waist under normal incident; and the transmitted THz pulses were recorded as function of time delay between THz pulse and optical probe pulses. The time domain THz pulses were then converted to frequency dependent spectrum by performing numerical FFT on individual terahertz pulses. The amplitude transmission of a sample is measured by taking the ratio of THz spectrum through sample to the reference. Optical pump beam is utilized to initiate photo-induced characteristic change in the samples which can be dynamically characterized by coherent THz spectroscopy.

III Ultrafast switching of surface plasmons resonances

To demonstrate the ultrafast switching of SPP resonances we fabricate two identical samples on two different substrates. The first sample used in this work was a 2D metallic hole array fabricated on semi-insulating (SI) GaAs with a carrier lifetime on the order of nanoseconds. The second sample used the same metallic hole array fabricated on a superlattice consisting of alternating layers of GaAs and ErAs nanoislands grown on semi-insulating (SI) GaAs. ErAs:GaAs superlattices have already proven to benefit many ultrafast applications such as THz photoconductive receivers, fast switchable THz metamaterials, etc[29,30]. Their carrier lifetime can be designed ranging from hundreds of femtoseconds to tens of picoseconds by changing the superlattice period[31].

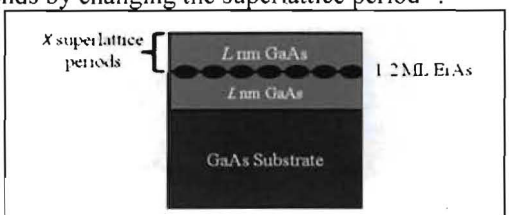

Fig. 1 Schematic diagram of ErAs:GaAs superlattice

Fig. 1 shows a generalized schematic diagram of ErAs:GaAs superlattice which is consisted of monolayer (ML) of self-assembled ErAs nanoislands embedded in a GaAs matrix. The ErAs nanoisland layers are separated by a thin GaAs layer of thickness L which defines the period of superlattices. The ErAs:GaAs substrate used in this work was grown by molecular-beam epitaxy (MBE) on <100> semi-insulating GaAs substrate. The ErAs nanoislands layer is grown at the same temperature as GaAs with a thickness of 1.2 ML. The carrier life time of the superlattice layer depends on the period L. Also, the thickness of the superlattice layer for our sample was 2 μm to assure complete absorbtion of the optical pump.

Both substrates have a direct bandgap across which carriers can be excited by 800 nm light. Standard photolithography was used to fabricate the aluminum (200-nm-thick) hole arrays on the substrates. A schematic cross-sectional view of the samples is shown in Fig. 2. The rectangular holes of dimension 50 μm × 25 μm were patterned in a square array with a lattice constant of 100 μm.

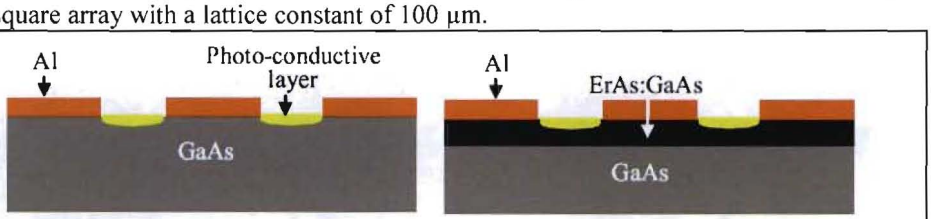

Fig. 2 Schematic cross-sectional view of the metallic hole array samples on GaAs and ErAs:GaAs substrates. The substrates in the hole areas, labeled "Photo-conductive layer," become conductive under optical illumination.

During the optical pump terahertz probe measurements the samples were placed at THz beam waist under normal incident. The sample size was 10 mm × 10 mm, large enough to cover 3.5-mm-diameter THz beam. The samples were illuminated with an optical excitation beam at an angle of ~10°. To obtain the optical switching, we compared the behavior of resonant THz transmissions through metallic hole array under various optical excitation fluences. The thickness of the metal is much thicker than the skin depth of metal at optical frequencies. Incident visible light interacts with the substrate only through the hole areas and generated photocarriers as shown by the yellow areas at Fig.2.

Figure 3(a) shows the THz transmission $|T(\omega)| = |E_{sam}(\omega)/E_{ref}(\omega)|$ through the metal hole array on GaAs substrate at various pump fluences normalized to the transmission of a blank unexcited GaAs reference slab. The dielectric constant of metals at THz frequency is much larger than the dielectric constant of dielectrics $|\varepsilon_2| \gg \varepsilon_1$. Thus, the resonance frequency of the fundamental SPP mode of the grating at normal incidence is approximately given by $f_{res} = c/\left(L\sqrt{\varepsilon_1}\right)$, where L is the period of the hole array, ε_1 is the dielectric constant of the substrate, and c is the speed of the light in vacuum. Transmission measurements show fundamental surface plasmon resonances of the [1, 0] mode around 0.8 THz, which is close to the theoretical prediction of 0.88 THz. Without optical excitation, the peak transmission at resonance is 37% relative to the blank unexcited GaAs slab. The transmission drops under photoexcitation because of the creation of a photoconductive layer on the top of the GaAs substrate as shown in Fig. 3.

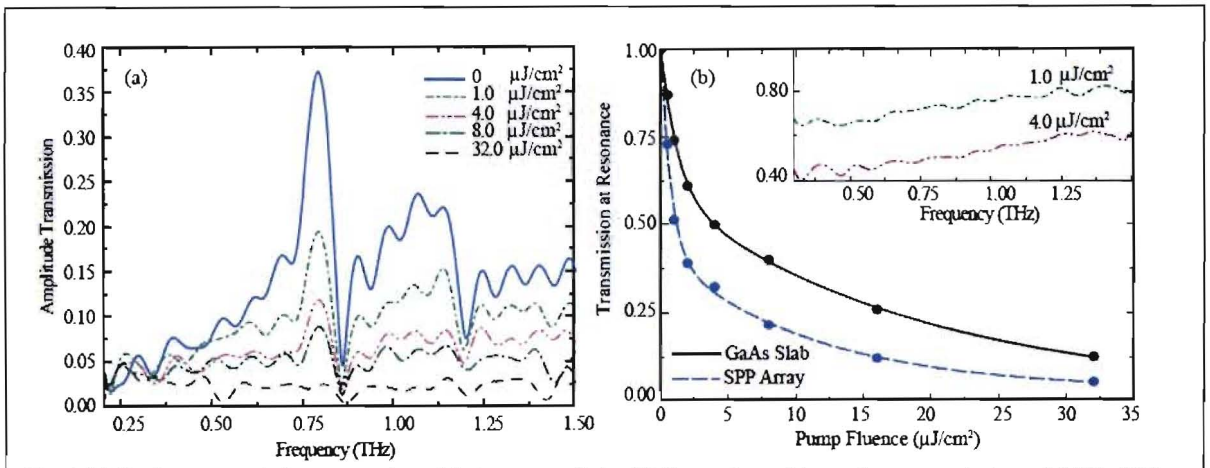

Fig. 3 (a) Terahertz transmission spectra through hole array on GaAs. (b) Comparison of the terahertz transmission at 0.8 THz (SPP Resonance) through the blank GaAs slab and the hole array on GaAs as a function of the pump fluence: Solid circles represent the measured data and the lines are the biexponential decay fittings. Inset shows the flat transmission through the GaAs slab.

The thickness of the photoexcited layer on GaAs for 800 nm light is ~0.8 μm. The DC conductivity of the photoexcited GaAs layer for a fluence of 16 μJ/cm^2 was estimated at about 200 (Ω-cm)$^{-1}$ and decays with time[31]. The transmission at the resonance drops to 7.5% with an excitation fluence of 8 μJ/cm^2. The intensity modulation depth can be defined as, $\left(T_0^2 - T_{Pump}^2\right)/T_0^2$ where T_0 and T_{Pump} are the amplitude transmission without and with pump. We obtained over 95% modulation depth with an optical fluence of 8 μJ/cm^2. We also performed THz transmission through a blank GaAs slab as a function of the pump fluence. Figure 3(b) shows the comparison of the fluence dependent transmission of metal hole array on GaAs (dotted lilne) and blank GaAs slab (solid line) at 0.8 THz. A bi-exponential decay function is used to fit the measured data. The normalized transmission through the photoexcited slab exhibited a broadband and flat attenuation as shown in the inset of Fig. 3(b). Measurements show that within the low fluence limit (in our case < 15 μJ/cm^2) the transmission amplitude of the hole array sample decays faster than the broadband transmission in the blank substrate. This suggests that SPP resonance damping plays an important role in modulation beyond simple propagation loss through the photoconductive layer. Apparently, only weak illumination is required for the photoconductive layer to damp the SPP resonance across the holes. However, at higher fluence the GaAs behaves as a metallic substrate and the THz transmission through metallic hole arrays and bare GaAs both suffer high attenuation. We have not noticed any pump dependent shift in the resonance frequencies. Due to the direct bandgap and higher mobility of photocarriers, GaAs requires low fluence for the complete switching compared to the fluence used in Ref. [26] for a grating on a silicon substrate.

The SPP sample on GaAs substrate does not show the recovery of the SPP resonance for hundreds on picoseconds. To demonstrate the switching recovery, we measured the THz transmission through metallic hole array fabricated on the ErAs:GaAs superlattice substrate. The ErAs:GaAs superlattice layer was 2 μm thick to ensure complete absorption of the incident 800 nm light and it had a designed carrier lifetime of ~8 ps. The fluence dependent THz transmission through the metal hole arrays on ErAs:GaAs is shown in Fig. 4(a). During these measurements the optical pump delay was carefully timed to ensure maximum modulation of the transmitted THz pulses. Fluence dependent measurements are similar to those of metal hole array on SI-GaAs. A thin conducting layer of the photoexcited layer damped the surface plasmon across the holes, diminishing the resonance amplitude. We obtained almost 88% modulation depth of the transmitted terahertz intensity when excited a pump fluence of 8 μJ/cm^2. Resonance amplitudes kept decreasing with increasing fluence until we observe a complete switch-off of the transmitted THz resonance for an optical fluence of ~32 μJ/cm^2.

The ultrafast switching recovery of the surface plasmon resonance in the metal hole array on the ErAs:GaAs superlattice substrate is demonstrated through the measurements of the THz transmission as a function of the time delay after the photoexcitation. The experimental results are shown in Fig. 4 (b) with an optical excitation fluence of 8 μJ/cm^2. It clearly reveals the annihilation and then fast recovery of the resonance at 0.8 THz (as well as the higher order resonances). Transmission shows a pronounced resonance before arrival of the optical pulses. It is then strongly attenuated within 1 ps after optical pulse arrival, but eventually recovers as the time delay increases.

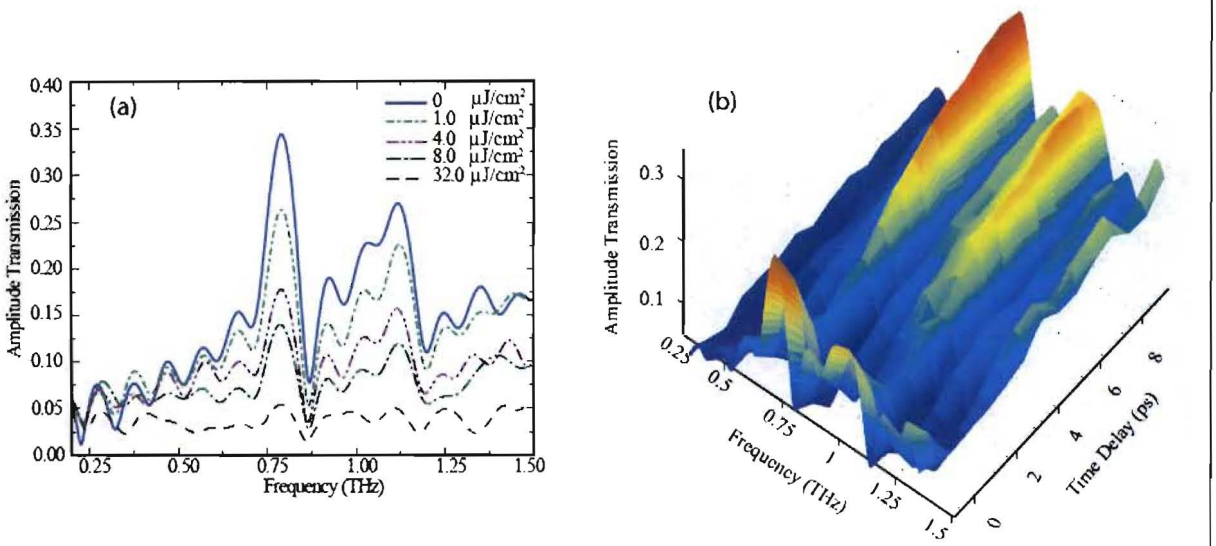

Fig. 4 (a) Resonant terahertz transmission spectra through a metallic hole array on an ErAs:GaAs superlattice substrate. Optical pump delay was carefully set to zero to obtain maximum modulation depth. (b) Pump delay dependent transmission spectra with an optical pump fluence of 8 μJ /cm².

Unlike bulk GaAs, the superlattice shows a fast carrier relaxation because ErAs nanoislands trap photocarriers immediately, long before they complete the recombination process. The measurement shows that the resonance recovery time is ~10 ps, approximately the carrier lifetime in the ErAs:GaAs superlattice. This fast recovery of the resonance demonstrates the ability of such metallic gratings to work as ultrafast modulators at room temperature. Shortening the carrier lifetime could further reduce this resonance recovery time.

The resonant THz transmission through the 2D metallic hole arrays usually reveals a Fano line shape due to the coupled contributions of the resonant and direct (non-resonant) transmissions. The Fano transmittance can be written as[20],

$$|T(\omega)|^2 = T_a + T_b\left(\left(1+\sum\frac{q_v}{\Delta\varepsilon_v}\right)^2 \Big/ \left[1+\left(\sum\frac{q_v}{\Delta\varepsilon_v}\right)^2\right]\right) \qquad (2)$$

where $\Delta\varepsilon_v = \left((\omega-\omega_v)/(\Gamma_v/2)\right)$, T_a is a slowly varying component associated with the direct transmission, and T_b is the contribution of a zero-order continuum that couples with the discrete resonance. Figure 5 shows the Fano fitting for the GaAs grating before and after photoexcitation with 8 μJ/cm^2 optical fluence. The Fano line shapes agree well with our measured fundamental resonances before and after the photoexcitation. The resonant state is characterized by the resonant frequency ω_v, linewidth Γ_v, and the Breit-Wigner-Fano coupling coefficient q_v. Fitting shows that the resonance frequency and linewidth remain unchanged with the optical excitation.

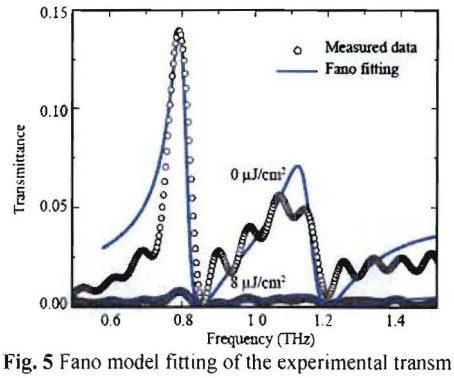

Fig. 5 Fano model fitting of the experimental transmittance.

The fitting parameters for the unexcited samples are: T_a=0.0001, T_b=0.0002; and for the photoexcited sample are T_a=0.00001, T_b= 0.0001. The other common parameters are q_1=23.9248, Γ_1=0.1224, ω_1=0.7732, q_2=17.2833, Γ_2=0.24, ω_2=1.082, q_3=13.3153, Γ_3=1.0, and ω_3=1.5. The excellent agreements between Fano fittings and the experimental results reveal the contribution of both resonant and direct transmission to the SPP resonances.

IV Dynamic switching between surface plasmon and localized surface plasmon resonances

Electromagnetic field enhancement due to resonant excitation of dipolar localized surface plasmons (LSPs) also occurs when electromagnetic waves impinge upon subwavelength metallic patch arrays[32-35] which are complimentary structure to the metallic hole arrays. In contrast to SPPs, the LSP resonance in the subwavelength geometries appears as a well-defined minimum in transmission with a central frequency primarily determined by the dimension of the particle and the dielectric function of boarding media. The coupling effect between SPPs and the localized modes have also been well explored recently[7, 36-37]. In this section, we present an active plasmonic film that allows instantaneous, large, and dynamic transitioning of the transmitted terahertz amplitude and phase by switching between the SPP and LSP resonances on a single integrated chip. Such plasmonic film was lithographically fabricated from silicon-on-sapphire (SOS) and is comprised of periodic arrays of metal patches and silicon holes. An evolution from a LSP to a SPP resonance reveals a large dynamic changeover effect and a giant phase shift (up to $\pi/2$).

The composite plasmonic film was patterned on a 350 μm thick undoped SOS substrate having a 500 nm thick epitaxial silicon layer. The sample is schematically illustrated in Figs. 6(a) and 6(b), where the Al patches and silicon holes are periodically fabricated using two-layer photolithography on a single chip. The 200 nm thick Al patches were first metallized on SOS and then the silicon holes adjacent to the patches were formed by reactive ion etching[38]. The resulting 78 × 25 μm^2 rectangular Al patches and 65 × 50 μm^2 rectangular silicon holes have the same periodicity of 100 μm. The dimensions of the patches and holes were designed to optimize overlapping between the LSP transmission dip and the SPP band-pass peak.

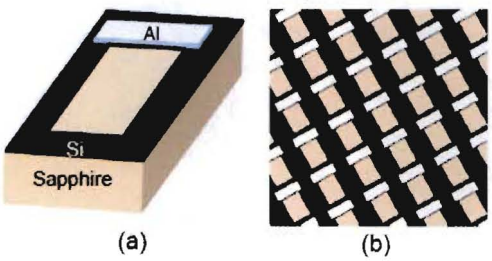

Fig. 6. Schematic of (a) a single unit cell, and (b) the periodic array comprising the composite plasmonic crystal.

The sample is measured using an optical pump THz probe spectrometer and the switching is obtained under optical excitation. In the absence of optical pumping, the silicon layer is highly transparent to the THz radiation and thin structured layer of silicon does not have evident affect on transmission while the THz propagating through samples. During measurements, the THz radiation was impinging on the sample at normal incident with the THz electric fields along the length of Al patch. The frequency dependent transmission of the sample was obtained by comparing the THz transmission through a bare sapphire substrate.

Figure 7 shows the resonant terahertz transmission through the composite structure with and without optical excitation. Without optical excitation, a well-defined transmission minimum occurs at 0.78 THz due to dipolar LSPs of the Al patches. The LSP resonance is also described through the relation $\omega_{LSP}/2\pi = (c/2L)\varepsilon_d^{-1/2}$, where c is the speed of light in vacuum, L is the length of the island axis parallel to the terahertz electric field, ε_d is the dielectric function of the substrate[34]. However, with an optical excitation of fluence 1.2 mJ/cm^2, the transmission is switched from band-stop to a band-pass with a characteristic transmission peak at 0.86 THz. Due to photo-doping, the silicon array becomes metallic and favors the resonant excitation of SPPs[20]. Such a SPP resonance is ascribed to the metal-

sapphire $[\pm 1,0]$ SPP mode with the relation $\omega_{SP}/2\pi = (c/p)[\varepsilon_m \varepsilon_{sphr}/(\varepsilon_m + \varepsilon_{sphr})]^{-1/2}$, where p denotes the lattice constant of the array, ε_m and ε_{sphr} and are the dielectric function of the photoexcited silicon and sapphire[20].

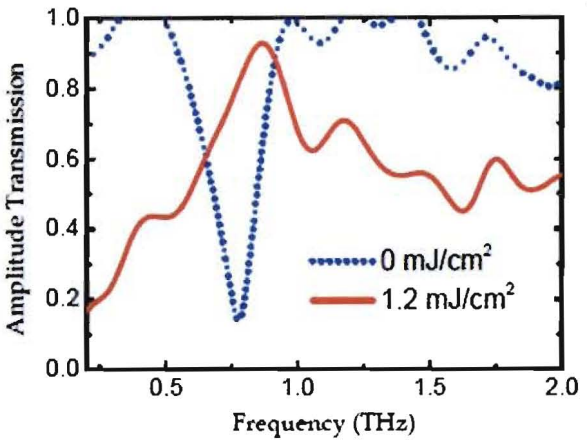

Fig. 7 Measured fundamental resonances at $\omega_{LSP}/2\pi$ (dotted curve) and $\omega_{SP}/2\pi$ (solid curve).

The measured characteristic transition between the LSP and SPP modes under various optical excitations is illustrated in Figs. 8(a) and 8(c), respectively, for the frequency-dependent amplitude transmission and the corresponding phase change. In order to tailor the offset between the LSP and SPP resonance frequencies, we intentionally rotated the chip about the normal of the array plane by 20° to modify the effective length of the patches and the geometrical parameters of the holes. Since the undoped silicon hole array does not support SPPs without optical excitation, only a dipolar LSP mode at 0.81 THz is observed[35], showing a band-stop resonance. With optical excitation, the dielectric function of silicon is modified due to photo-generated free carriers, and the LSP resonance gradually diminishes with a broader linewidth and a less pronounced transmission minimum. The further increase in optical excitation alters the dielectric function of silicon such that it begins to present metallic properties. Thus, the Al patches can be electrically connected by the metallic silicon film and the charges confined to the Al patches will be redistributed over the whole film surface. As a result, the LSP minimum gradually disappears and the SPP resonance peak appears almost at the same frequency. With strong optical excitation, the silicon film along with the Al patches form a metallic hole array, exhibiting an overall band-pass type SPP response. We also observe that the resonance frequency of the SPP mode slightly red-shifts with a narrower linewidth due to reduced damping rate of SPPs. At 1.0 mJ/cm^2 optical excitation, the resonance is located around 0.83 THz, originating from the metal-sapphire $[\pm 1,0]$ SPP mode.

To gain further insight, two-dimensional finite-element simulations using CST Microwave Studio were carried out to model the transition characteristics between the LSP and SPP resonances. In the simulation, the sapphire substrate is treated as a lossless dielectric with ε_{sphr} = 9.61 and the Al film is modeled as a Drude metal. The simulation results shown in Fig. 8(b) reproduce very well the characteristic amplitude transition between the two observed resonance modes. The transmission response of the composite structure undergoes three characteristic states, namely, the LSP, SPP, and intermediate states. The LSP state occurs when optical excitation is not yet applied and the chip behaves as an array of the 78 × 25 μm^2 Al patches. The electric field distribution of the composite structure is calculated at the resonance frequency and illustrated in Fig. 8(e). It indicates that the electric field is mainly confined around the Al patches due to dipolar LSPs and their coupling between adjacent patches.

The intermediate response state takes place at 0.4 mJ/cm^2 optical excitation where a nearly flat response is observed in the transmission, i.e. the signature of the LSP mode disappears while the SPP resonance peak has not yet been established. As optical excitation approaches 0.4 mJ/cm^2, the real part of dielectric function ε_{rm} of silicon is gradually altered from positive to negative. Thus, the LSP minimum gradually broadens and disappears due to damping, a result of ohmic losses in the silicon layer. Meanwhile, the resonance shifts to lower frequencies due to modification in the dielectric function of the silicon layer [11]. It is interesting to note, although the silicon layer has

acquired metallic properties by having a negative real part of dielectric function ε_{rm} at 0.4 mJ/cm^2 optical excitation, the SPP resonance is not yet established. This is because the thickness of the silicon layer also needs to be larger than one third of the skin depth[6] to support the SPP resonance. At 0.4 mJ/cm^2 optical excitation, the skin depth of silicon is 3.96 μm at the resonance 0.81 THz, nearly eight times of the layer thickness. It thus does not support the SPP resonance. Nevertheless, as illustrated in Fig. 8(f), a weak SPP electric field appears confined in the silicon holes, while the LSP signature disappears.

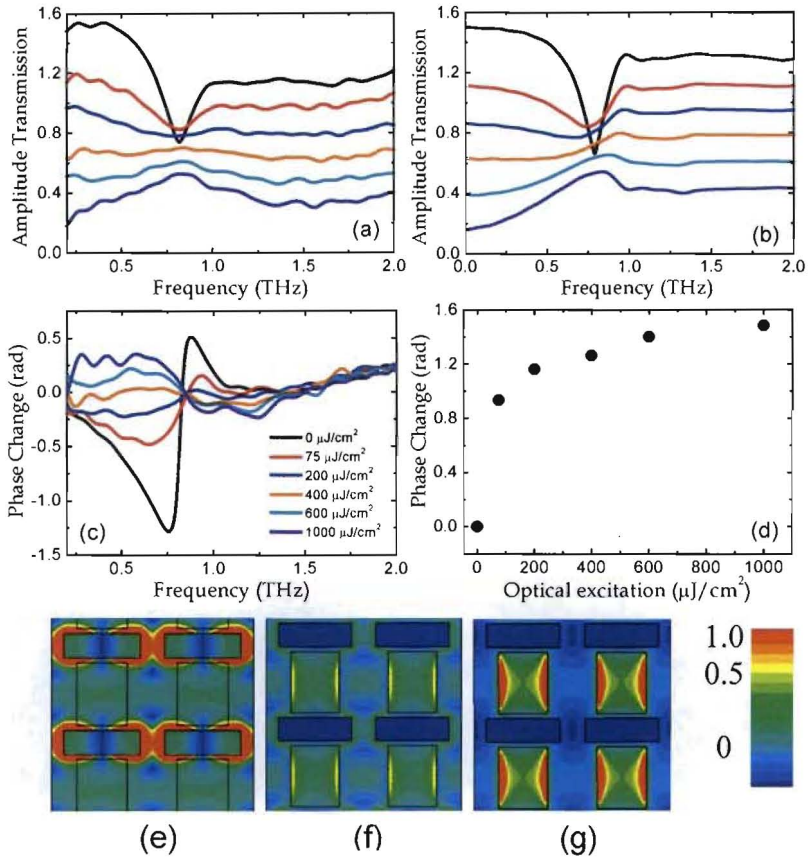

FIG. 8. Frequency-dependent amplitude transmission at various optical excitations: (a) experimental results, and (b) simulation results. The measurements and simulation results for different optical excitations are vertically shifted by 0.5 each for clarity. (c) Measured corresponding phase change. (d) Optical excitation dependent phase change at 0.76 THz. Electric field distribution at resonance frequencies under various optical excitations: (e) 0, (f) 400, and (g) 1000 μJ/cm^2.

When optical excitation is increased above 0.4 mJ/cm^2, the silicon layer exhibits improved metallic properties that lead to reduced skin depth. The SPP state begins to emerge with a resonance peak, which red-shifts and narrows in linewidth with increasing optical excitation. Although the thinner skin depth in the photo-excited semiconductors was found to reduce the effective size of the holes, the effect on the transmission amplitude is negligible when the silicon layer is sufficiently thin[25, 32], as in this case. The high density of photo-generated free carriers in the silicon layer enables a relatively high ratio of the real to imaginary parts of dielectric function $-\varepsilon_{rm}/\varepsilon_{im}$, which plays a crucial role in the improved resonance enhancement at the maximum optical excitation 1.0 mJ/cm^2 [39]. A strong electric field due to SPPs is now revealed in the holes, as shown in Fig. 8(g). The observed resonance shift and linewidth narrowing effects mainly originate from the improved metallic properties; this leads to higher magnitudes of the silicon dielectric function and less damping.

Along with the amplitude transition between the dipolar LSP and SPP modes, the transmission phase undergoes a strong modulation. Figure 8(c) depicts the measured characteristic evolution of phase change under various optical

excitations at 0.76 THz. Due to the Kramers-Kronig relation, the transmission amplitude and phase change are dependent on each other. At 0.76 THz, the amplitude shows minimum modification but the phase undergoes a maximum change, as shown in Fig. 8(d). At 0.81 THz, however, the phase intersects for various optical excitations, but is accompanied with a maximum amplitude variation. Under 1.0 mJ/cm^2 optical excitation, a maximum phase shift of $\pi/2$ is achieved, thus showing great potential for large dynamic phase modulation at terahertz frequencies[40]. To further improve switching contrast, sharper SPP resonances can be achieved by use of semiconductors of higher carrier mobility, for example, GaAs. It is also possible to achieve ultrafast switching between the LSP and SPP modes by implementing ErAs:GaAs nanoisland or any other epitaxial films that have ultrashort carrier recombination time.

V Conclusion

In conclusion, we have demonstrated ultrafast switching of the SPP resonance on a two dimensional metallic hole arrays. ErAs:GaAs sample shows an intensity modulation depth of ~88% with an optical pump fluence of 8 μJ/cm^2, and SPP resonance recovery (switching) time of ~10 ps. Our data suggests that SPP resonance damping enhances modulation in the low fluence limit compared to simple propagation loss in the photoconductive layer. We point out that our hole array on ErAs:GaAs requires an order of magnitude lower optical fluence compared to the work in Ref. 18 and room temperature operation supports future applications. In addition, we demonstrate a composite terahertz plasmonic crystal that exhibits large a dynamic transition between the dipolar LSP and SPP resonances under optical excitation. The reversal in transmission amplitude and up to $\pi/2$ phase shift observed in the composite plasmonic crystal make it promising for optical changeover switching and large dynamic phase modulation, as well as active plasmonic device applications.

References:

1. T. W. Ebbesen, H. J. Lezec, H. F. Ghaemi, T. Thio, and P. A. Wolff, *Nature (London)* **391**, 667 (1998).
2. D. Qu, D. Grischkowsky, and W. Zhang, Opt. Lett. **29**, 896 (2004).
3. H. Cao and A. Nahata, Opt. Express **12**, 1004 (2007).
4. D. Qu and D. Grischkowsky, Phys. Rev. Lett. **93**, 196804 (2004).
5. T. Matsui, A. Agrawal, A. Nahata, and Z. V. Vardeny, Nature **446**, 517 (2007).
6. A. K. Azad and W. Zhang, Opt. Lett. **30**, 2945 (2005).
7. H. Raether, *Surface plasmons on smooth and rough surfaces and on gratings* (Springer-Verlag, Berlin, 1988).
8. E. Ozbay, Science **311**, 189 (2006).
9. A. K. Azad, J. Dai, and W. Zhang, Optics Letters, **31**, 634 (2006).
10. H.-T. Chen, W. J. Padilla, J. M. O. Zide, A. C. Gossard, A. J. Taylor, and R. D. Averitt, Nature **444**, 597 (2006).
11. H. –T. Chen, J. F. O'Hara, Abul K. Azad, A. J. Taylor, R. D. Averitt, D. B. Shrekenhamer and W. J. Padilla, Nature Photonics, **2**, 295(2008).
12. H. Nemec, P. Kuzel, L. Duvillaret, A. Pashkin, M. Dressel, and M. T. Sebastian, Opt. Lett. **30**, 549 (2005).
13. L. Fekete, F. Kadlec, P. Kuzel, and H. Nemec, Opt. Lett. **32**, 680–682 (2007).
14. S. Savelev, A. L. Rakhmanov, and F. Nori, Phys. Rev. Lett. **94**, 157004 (2005).
15. T. Thio, H. F. Ghaemi, H. J. Lezec, P. A. Wolff, and T. W. Ebbesen, J. Opt. Soc. Am B **16**, 1743 (1999).
16. D. E. Grupp, H. J. Lezec, T. W. Ebbesen, K. M. Pellerin, and T. Thio, Appl. Phys. Lett. 77, 1569 (2000).
17. M. A. Ordal, L. L. Long, R. J. Bell, S. E. Bell, R. R. Bell, R. W. Alexander, Jr., and C. A. Ward, Appl. Opt. **22**, 1099 (1983).
18. L. Martín-Moreno, F. J. García-Vidal, H. J. Lezec, A. Degiron, and T. W. Ebbesen, Phys. Rev. Lett. **90**, 167401 (2003).
19. H. A. Bethe, Phys. Rev. **66**, 163–182 (1944).
20. W. Zhang, A. K. Azad, J. Han, J. Xu, J. Chen, X. –C. Zhang, *Phys. Rev. Lett.* **98**, 183901 (2007).
21. H. –T. Chen, H. Lu, A. K. Azad, R. D. Averitt, A. C. Gossard, S. A. Trugman, J. F. O'Hara, and A. J. Taylor, *Opt. Express*, **16**, 7641 (2008).
22. H. –T. Chen, W. J. Padilla, J. M. O. Zide, A. C. Gossard, A. J. Taylor, and R. D. Averitt, *Nature* **444**, 597 (2006).
23. J. G. Rivas, P. H. Bolivar, and H. Kurz, *Opt. Lett.* **29**, 1680 (2004).
24. C. L. Pan, C. F. Hsieh, R. P. Pan, M. Tanaka, F. Miyamaru, M. Tani, and M. Hangyo, *Opt. Express*, **13**, 3921 (2005).
25. E. Hendry, F. J. Garcia-Vidal, L. M. Moreno, J. G. Rivas, M. Bonn, A. P. Hibbins, and M. J. Lockyear, *Phys. Rev. Lett.* **100**, 123901 (2008).
26. E. Hendry, M. J. Lockyear, J. G. Rivas, L. Kuipers, and M. Bonn, *Phys. Rev. B* **75**, 235305 (2007).
27. L. Xu, X. –C. Zhang, and D. H. Auston, Appl. Phys. Lett. 61, 1784 (1992).
28. A. K. Azad, R. P. Prasankumar, D. Talbayev, A. J. Taylor, R. D. Averitt, J. M. O. Zide, H. Lu, A. C. Gossard, and John F. O'Hara, *Appl. Phys. Lett.* **93**, 121108 (2008).
29. J. F. O'Hara, J. M. O. Zide, A. C. Gossard, A. J. Taylor, and R. D. Averitt, Appl. Phys. Lett. **88**, 251119 (2006).

30. H.-T. Chen, W. J. Padilla, J. M. O. Zide, S. R. Bank, A.C. Gossard, A. J. Taylor, and R. D. Averitt, Opt. Lett. **32**, 1620 (2007).
31. R. P. Prasankumar, A. Scopatz, D. J. Hilton, A. J. Taylor, and R. D. Averitt, Appl. Phys. Lett. **86**, 201107 (2005).
32. E. J. Smythe, E. Cubukcu, and F. Capasso, Opt. Express **15**, 7439 (2007).
33. C. L. Haynes, A. D. Mcfarland, L. Zhao, R. P. Van Duyne, and G. C. Schatz, J. Phys. Chem. B **107**, 7337 (2003).
34. X. Lu, J. Han, and W. Zhang, Appl. Phys. Lett. **92**, 121103 (2008).
35. X. Lu and W. Zhang, Appl. Phys. Lett. **94**, 181106 (2009).
36. B. I. Greene, John F. Federici, D. R. Dykaar, A. F. J. Levi, and L. Pfeiffer, Opt. Lett. **16**, 48 (1991).
37. B. Ferguson and X.-C. Zhang, Nat. Mater. **1**, 26 (2002).
38. A. K. Azad, Y. Zhao and W. Zhang, *Appl. Phys. Lett.* **86**, 141102 (2005).
39. A. K. Azad, Y. Zhao, W. Zhang, and M. He, Opt. Lett. **31**, 2637 (2006).
40. H.-T. Chen, W. J. Padilla, M. J. Cich, A. K. Azad, R. D. Averitt, and A. J. Taylor, *Nat. Photon.* **3**, 148 (2009).